

A Bifurcation of a Two-Dimensional Symmetric Flapping Model

飯間 信 柳田 達雄
Makoto IIMA* and Tatsuo YANAGITA†

*Nonlinear Studies and Computation, Research Institute for Electronic Science,
Hokkaido University, Sapporo 060-0812, Japan*

(Dated: September 7, 2001)

A two-dimensional symmetric flapping model is studied in terms of the bifurcation. This model consists of two wings attached together at a hinge, and the flapping motion of the wings is symmetric with respect to the horizontal line. The center of mass of this model can move according to the lift generated by an interaction of the wing and vortices separated from boundary layer. The bifurcation parameter is a time scale of the diffusion, which is simplified to contrast the transition of the type of the motion. Bifurcation diagram shows that there are unstable regions for a steady flapping motion of zero-mean velocity, and that there is a region where two types of a steady stable flapping motion coexist. We illustrate these types of the motion.

I. INTRODUCTION

The problem of a motion of a body interacting with fluid is familiar to us: a coin motion dropped in water[1, 2], insect flight[3–7], and the flapping flag in wind[8]. In the case of two-dimensional inviscid fluid without vorticity, the motion of the body in fluid is described by ordinary differential equations [9, 10]. In these cases listed above, however, their various motion should be understood as a vortex-body interaction: the motion of a body is dominated by an interaction between the vortices separated from boundary layer (separation vortex) and the body.

In the case of the insect flight, they can not even sustain their weight without such interaction[3]. Experimental studies using a real insect and a mechanical model [4, 5, 11–13], and numerical simulations[14, 15] show that the separation vortex from the leading-edge produces an extra lift. The lift-enhance mechanism, called delayed stall, is proven to exist in a real life insects, but the detail of the mechanism has not been understood.

An analysis of a simple flapping motion in two-dimensional fluid which is calculated by direct numerical simulation (DNS) reveals some aspects of the vortex-body interaction in a flapping flight such as dipole jet emission during one type of hovering[16], and a frequency selection mechanism in a uniform flow[17].

Coin motion falling in fluid is also determined by the vortex-body interaction. Three-dimensional experiment[1] and pseudo two-dimensional experiment[2] show that separation vortices interacting with the body is a critical element for determining their motion. In the case of flapping flag, separation vortex is also observed[8].

Here we focus our attention on the motion of a body with flapping wings in two-dimensional fluid [18]. The motion of the center of mass (CM) due to vortex-wing interaction is considered. Within the authors' knowledge, there is no study of a flapping model considering the motion of CM. The condition of the free motion of CM permits us to consider stability, as well as the effect of the body inertia[19], where the ratio of fluid density and the inertial mass of the body in a non-dimensional form is the critical parameter to determine the type of the motion as well as the coin motion[1, 2].

Our question considered here is simple: what happens to the motion of CM if the flapping motion is symmetric, there is no gravity, and any kind of airspeed is disregarded? The answer appears trivial, because symmetric flapping motion seems to give symmetric lift contribution. Sunada *et. al.* calculated a vortex-wing interaction without the dynamics of separation vortex,

*Electronic address: makoto@aurora.es.hokudai.ac.jp; URL: <http://aurora.es.hokudai.ac.jp/~makoto>

†Electronic address: yanagita@aurora.es.hokudai.ac.jp; URL: <http://aurora.es.hokudai.ac.jp/~yanagita>

and state that there is no mean lift in a symmetric flapping[20]. Wang performed DNS of the flow following a flapping elliptic wing in uniform flow. Her result shows that the lift function of time is symmetric if the angle of attack is zero[17]. On the contrary, we found that the symmetry of lift production can be broken due to the vortex-wing interaction [18].

In this paper, we study this symmetry-breaking phenomenon in terms of the bifurcation. In section II, the detail of the model is described. We briefly review a typical vortex-body interaction in section III. The bifurcation diagram is shown in section IV, and we show the dynamics of the two flapping phases in section IV C.

II. THE TWO-DIMENSIONAL FLAPPING MODEL

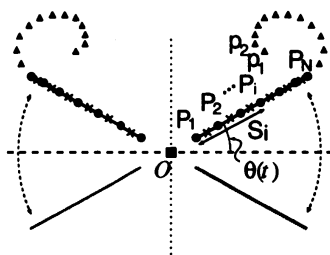


FIG. 1: The geometry of our model. The wings are represented by point vortices drawn as circles, and the body is represented by the square located at the hinge O . Slip boundary conditions are required at the point midway between each pair of adjacent boundary vortices (represented by crosses). The boundary vortices at the outer edges of the wings become detached, thereby becoming separation vortices (represented by triangles). At each time step one vortex is shed from each wing in this manner. Mirror symmetry with respect to the vertical center line represented by the broken line for both the flow and the wings is assumed.

Our flapping-flight model “butterfly” has wings represented by two rigid lines swinging on a hinge in two dimensional space, as shown in fig.1. For simplicity, we assume mirror symmetry for the motion of the wing and fluid with respect to the vertical center line and that the “butterfly” can move in the vertical direction only. The fluid around the wing is assumed to be incompressible and inviscid, but it is possible for vortices to be shed from the outer edge of each wing.

In order to model separation vortices, we used a discrete vortex method [21, 22], in which fluid motion and flow on the wings are approximated using vortex blobs. A single vortex blob at $\mathbf{x} = (x_0, y_0)$ induces the flow $(u(x, y), v(x, y)) = (-\frac{\Gamma(y-y_0)}{2\pi(\tau^2+\delta^2)}, \frac{\Gamma(x-x_0)}{2\pi(\tau^2+\delta^2)})$, where Γ is the circulation of the vortex, $r = \sqrt{(x-x_0)^2 + (y-y_0)^2}$, and δ is a smoothness parameter. For the details of the model, see ref. [19].

We note that this model implements a cut-off viscosity. Due to viscosity, the size of each vortex gradually grows, while the total circulation it possesses is preserved. This effect of viscosity can be implemented in a discrete vortex method in several ways[23]. Our purpose is to isolate the salient feature of the bifurcation, not to simulate an accurate fluid dynamics by a flapping motion. Thus we simplify the core-spreading dynamics of a separation vortex as follows. In our model, each separated vortex is shed from a wing at a particular time. Then, we define a characteristic “lifetime” of separated vortices T_{life} . We consider that the radius of the vortex suddenly becomes infinite when $\tau = T_{\text{life}}$, where τ is the length of time after which the vortex comes into existence; $\delta(\tau) = \delta_0(\tau < T_{\text{life}}); \infty(\tau > T_{\text{life}})$. Changing the effect of the separated vortices by considering different values of the lifetime, we can show that the interaction between the separated vortices plays an important role in the symmetry breaking.

Here we have used parameters corresponding to a butterfly [24]: wing mass $m = 3.5 \times 10^{-6}$ kg, body mass $M = 6.0 \times 10^{-5}$ kg, wing length $l = 3.0 \times 10^{-2}$ m, hinge-wing distance $l_d = 5.0 \times 10^{-3}$ m, period of flapping cycle $T = 0.1$ s. To evaluate the two-dimensional air density is not straightforward because of the difference between this two-dimensional model and real butterfly in three-dimensional space. Here, we used the parameter $\rho = 7.0 \times 10^{-3}$ kg/m². The

two-dimensional density itself, however, is not a critical parameter to determine the behavior of “butterfly”, which is characterized by a nondimensional number χ defined and discussed in [19].

For the time integration, the 4th order Runge-Kutta method and the Euler method with time step $\Delta t = 1.0 \times 10^{-4}$ (s) is used to calculation flow due to the wing flapping and the motion of the center of mass, respectively. We checked that the result does not depend significantly on Δt , N , and δ_0 . The value of simulation parameters Δt , N , and δ_0 used in the following sections are 1.0×10^{-4} , 50, and 1.0×10^{-4} , respectively. The flapping is assumed to be characterized by a sinusoidal function $\theta(t)$, which represents the angle made by each wing with respect to the horizontal line intersecting the hinge: $\theta(t) = \Delta\theta \cos(2\pi t/T)$ where $\Delta\theta = 0.36 \times 2\pi$.

In order to concentrate our attention on the bifurcation, mechanism, we consider the case without a gravitational force.

III. A SYMMETRY-BREAKING CASE

In this section, we briefly illustrate two typical cases of the result of the simulation using a nondimensional number $\eta \equiv T_{\text{life}}/T$. For the detail of the dynamics described in this section, see ref. [18].

The dynamical interaction between separated vortices and the wing shows asymmetric lift production in one case, $\eta = 1.0$, while we only see a trivial symmetric lift production in the other case, $\eta = 0.25$ (fig.2(a) and fig.2(b)).

In the case of $\eta = 0.25$, the generation of the coherent vortices during flapping motion is symmetric, as shown in fig.3. On the other hand, in the case of $\eta = 1.0$, asymmetric generation of the lift force has been observed, as shown in fig.2(b). The most characteristic dynamics is observed in the second downstroke. A coherent vortex V_2 generated in the first upstroke remains under the wing during the production of the coherent vortex V_3 created by the second downstroke (fig.4(c)). As a result, V_3 and V_2 together induce stronger outer flow around the wing. This flow generates a larger upward lift force.

Once the body attains a sufficiently large velocity, the distance between a wing and the coherent vortex it sheds in each downstroke becomes much shorter than the distance between this wing and the coherent vortex it sheds in the upstroke. As a result, $L(t)$ becomes asymmetric, unlike in the case of $\eta = 0.25$ (fig.2(a) and fig.2(b)). Through this mechanism, the center of mass of the “butterfly” moves asymmetrically despite the symmetric nature of the flapping, and the direction of its overall motion is determined by the direction in which the wings initially flap.

The symmetry-breaking mechanism requires two coherent vortex interacting with fluid. Since the number of the coherent vortex is controlled by η , we can expect a sharp transition from the state of the symmetric lift production to the state of the asymmetric lift production as η is increased. Fig.5 shows the averaged lift in the period $[T, 2T]$ as a function of $\eta \in [0, 2.0]$. The averaged lift shows a transition at $\eta = \eta_0 \simeq 0.62$. When $\eta < \eta_0$, the averaged lift is very small compared to the averaged lift in the case of $\eta > \eta_0$. Two typical dynamics in the first several periods, each of which is discussed above, corresponds to the case of $\eta < \eta_0$ and the case of $\eta > \eta_0$, respectively.

Fig.5 also shows that this model gives qualitatively only two state. In other words, even if two or more coherent vortex (of finite radius) are allowed to exist, the symmetry-breaking mechanism is essentially the same.

The number of the coherent vortex is roughly estimated by $[T_{\text{life}}/2T] = [\eta/2]$, because a half stroke (upstroke or downstroke) produces one coherent vortex. If $\eta < 0.5$, no coherent vortex can include all the separation vortices produced during a half stroke, because the lifetime of separation vortex is so short that some separation vortices included in a coherent vortex disappears (precisely, the radius of them is infinite). Such imperfect coherent vortex do not work effectively for inducing flow. The graph in fig.5 shows that in such case, the symmetric lift production is not broken in the second period.

On the other hand, if $\eta > 1.0$, there is roughly more than two coherent vortices which can work for lift production. Although the effect of the extra vortex is shown as a concave around $\eta = 1.5$, it is not significant compared with the change at $\eta = \eta_0$. Therefore extra coherent vortices do not play a critical role.

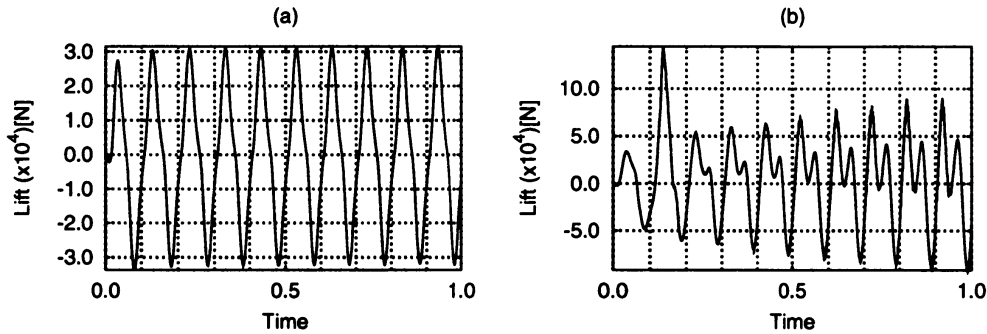


FIG. 2: The vertical lift force as a function of time. (a) In the case of $\eta = 0.25$, symmetrical lift generation is observed. (b) In the case of $\eta = 1.0$, asymmetrical generation of the lift force is found. This creates directed motion of the body despite the symmetrical nature of flapping.

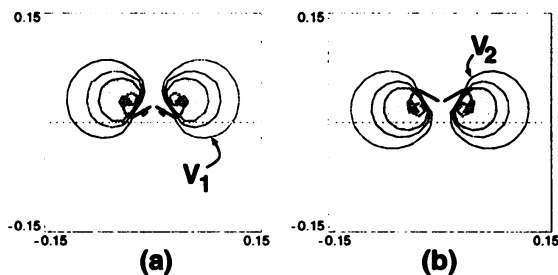


FIG. 3: Snapshots of the configuration of separated vortices and the wings in the case of $\eta = 0.25$. The separated vortices and streamlines are indicated by dots and contour lines, respectively. The two straight lines represent the wings. (a) $t=(5+3/8)T$: the beginning of the first downstroke. Separated vortices form a coherent vortex V_1 , which generates an upward vertical force. (b) $t=(5+7/8)T$: during the first upstroke. A coherent vortex V_2 is formed, and generates a downward force. In this case, symmetric lift generation is observed (see fig.2(a)).

In the region $0.5 < \eta < 1.0$, there are one perfect coherent vortex and one imperfect coherent vortex. The perfect one works for lift production fully, while imperfect one does not. The result that the critical value is $\eta \simeq \eta_0 = 0.62$ means that the existence of such secondary vortex, even if it is imperfect, is essential for the symmetry-breaking dynamics.

Lastly, we note that the case $\eta = 2.0$ corresponds to the case of inviscid fluid. Thus the symmetry-breaking is not the artifact due to our model viscosity.

IV. BIFURCATION

In this section, we study the stability of this model. As shown in section III, the cut-off viscosity is useful to characterize the vortex-wing interaction. A nondimensional parameter, η , is relevant to control the number of coherent vortex. Using η , we construct a bifurcation diagram. We found a more complicated structure of stable state in the case of $\eta < \eta_0$, while the dynamics in the second period appears to be a simple symmetric lift generation.

A. Existence of steady states

1 Convergence

First of all, we prove the existence of the steady state of this model. Fig.6 shows mean velocity in one period $\langle V \rangle_t \equiv \frac{1}{T} \int_t^{t+T} V dt$ for $\eta = 0.25, 0.5, 0.6, 0.7$ and 1.0 . Their convergence

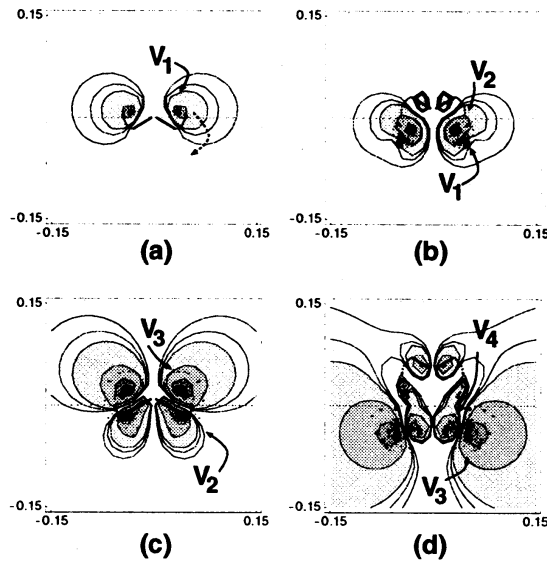


FIG. 4: Same as fig.3 but $\eta = 1.0$. (a) $t=3/8T$: the beginning of the first downstroke. Separated vortices form a coherent vortex V_1 , which generates an upward vertical force when it is above the wing. The broken arrow indicates the path of V_1 , which turns around and moves under the wings. (b) $t=7/8T$: during the first upstroke. A coherent vortex V_2 is formed and remains under the wing due to the flow induced by V_1 . (c) $t=11/8T$: the second downstroke. A coherent vortex V_3 is formed by the second downstroke, and V_2 induces stronger outward flow around the wing, which produces larger upward lift. (d) $t=17/8T$: the body is accelerated in the second downstroke, and moves to a higher position. A coherent vortex V_4 is formed in the second upstroke.

is attained in a practical sense when $t > 30T$. It should be noted that the mean velocity in the first periods does not correspond to the terminal velocity. The difference of the shape of $\langle V \rangle_t$ between the case of $\eta = 0.5$ and the case of $\eta = 0.6$ can not be discerned when $t < 5T$, while the limit of $\langle V \rangle_t$ for $\eta = 0.5$, about 0.9, is qualitatively different from the case $\eta = 0.6$: its limit is 0.0.

This case shows that the behavior of this model is not so simple, in spite of the high-symmetry this model possesses. This model has stable steady state, but the relation between the stable steady state and the typical dynamics is not straightforward: the stable steady state characterized by non-zero velocity can not always be obtained by the symmetry-breaking mechanism explained in sec.III, which is clearly shown by the case $\eta = 0.5$. Therefore, a further study about stable steady state is necessary for understanding this model, besides the analysis of typical dynamics gives prescribed forms of a nontrivial vortex-wing interaction.

The stable steady state can be described by velocity V and the circulation of a wing Γ . For this model, the stable steady state corresponds to a stable steady flapping state (SSFS) with period T .

2 Independence of initial phase

Next, we check the initial-phase dependency for SSFS. We performed simulations for the set of initial conditions \mathcal{S}_{in} :

$$\mathcal{S}_{\text{in}} = \{\theta_i(t) | \theta_i(t) \equiv \Delta\theta \cos(2\pi t/T + \phi); \phi = \frac{2\pi i}{N} (i = 0, 1, \dots, N); N = 10\}, \quad (4.1)$$

where $\theta_i(t)$ is the flapping angle.

We show the trajectory $T_{\eta, \phi}$ in the phase space defined by the circulation of the wing and the velocity

$$T_{\eta, \phi} \equiv \{(x, y) | x = \Gamma(t); y = V(t); t \in [29T, 30T]\}, \quad (4.2)$$

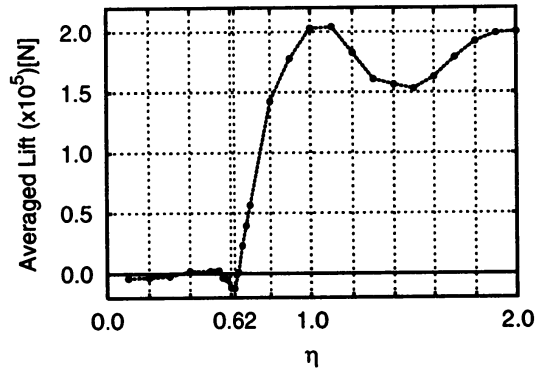


FIG. 5: Averaged lift in the period $[T, 2T]$: $\frac{1}{T} \int_T^{2T} L(t) dt$. As η increase, more coherent vortices of finite radius coexist. A transition is found at $\eta \simeq 0.62$. In case of $\eta > 1.0$, the average lift does not show a qualitative difference, although a reduce is observed around $\eta = 1.5$.

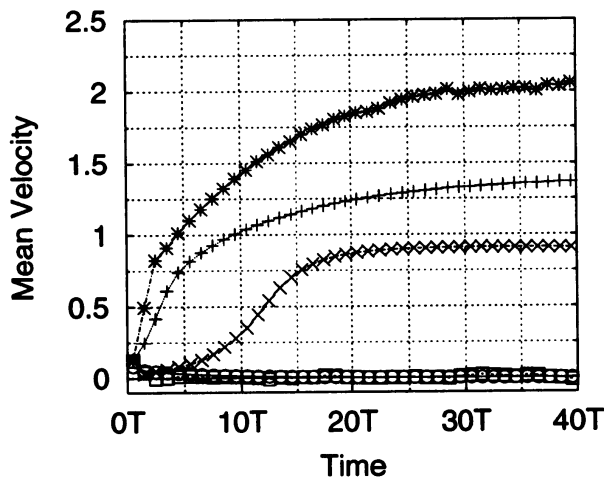


FIG. 6: Mean velocity function $\langle V \rangle_t$ for $\eta = 0.25$ (open circle), 0.5 (cross), 0.6 (open square), 0.7 (plus), and 1.0 (star). When $t > 30T$, $\langle V \rangle_t$ is almost constant.

where functions $\Gamma(t)$ and $V(t)$ depend on η and ϕ . If SSFS is an attractor of the model, the trajectory converges to one or several closed curve(s).

In fig.7, two types of SSFS are shown. In case of $\eta = 0.6$, all the initial condition (4.1) gives the same SSFS S_1 , which means that all the trajectory $T_{\eta, \phi \in S_{in}}$ converges to S_1 . Moreover, S_1 is symmetric to itself with respect to the origin: again, the symmetry is not broken in this case. On the other hand, in case of $\eta = 1.0$, two SSFS, S_2 and S_3 , are observed. Because changing ϕ into $\phi + \pi$ is equivalent to the mirror transform with respect to the horizontal line, S_2 and S_3 are symmetric to each other with respect to the origin.

Therefore, it is shown that this model gives one or more SSFS depending on the non-dimensional parameter η . In the next subsection, we draw the bifurcation diagram.

B. Bifurcation diagram

Because this model gives a SSFS, we can draw a diagram of the SSFS. This diagram shows the structure of the SSFS.

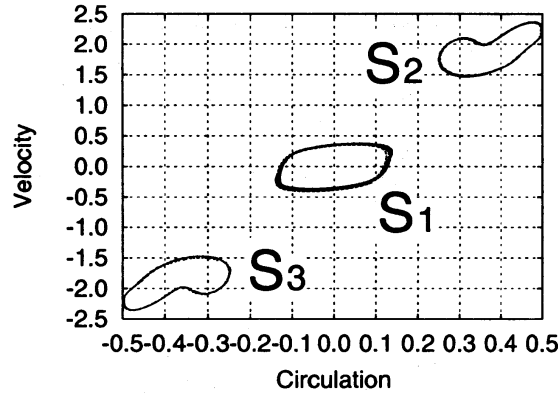


FIG. 7: Plot of $T_{\eta=0.6, \phi}$ (S_1) and $T_{\eta=1.0, \phi}$ (S_2 and S_3). Initial phase is changed according to (4.1). In case of $\eta = 0.6$, all the initial phases result in a unique SSFS. In case of $\eta = 1.0$, initial phases separates into two groups, both of which are symmetric with respect to the origin.

1 The method

To construct the diagram, we need SSFS for a given η . We used two kinds of simulation to obtain SSFS. One is $T_{\eta=\text{const.}, \phi}$ (defined in (4.2)) for the range $0.20 \leq \eta \leq 2.0$. We regard SSFS as the trajectory in $[29T, 30T]$, and characterize it by its mean value of the velocity. We plot the absolute value of the mean velocity $|\langle V \rangle_{t=29T}| \equiv \bar{V}$ as a function of η .

The other is the trajectory of $T_{\eta=\eta(t), \phi}$ where $\eta(t)$ is a slow-changing function defined as followings:

$$\eta(t) = \begin{cases} \eta_1 & (0 < t < t_1), \\ \eta_1 + \frac{\eta_2 - \eta_1}{t_2 - t_1}(t - t_1) & (t_1 \leq t < t_2), \\ \eta_2 & (t_2 \leq t < t_3), \\ \eta_2 + \frac{\eta_3 - \eta_2}{t_3 - t_2}(t - t_2) & (t_3 \leq t < t_4), \\ \eta_3 & (t_4 \leq t < T_{\text{end}}), \end{cases} \quad (4.3)$$

where T_{end} is the simulation time (see fig.8).

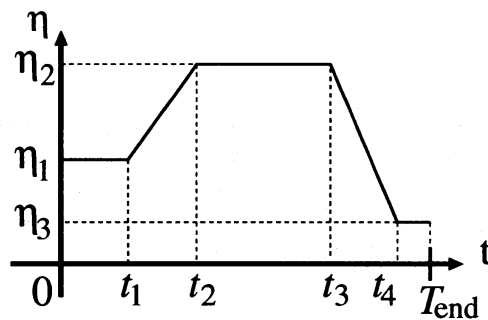


FIG. 8: Plot of the function $\eta(t)$.

We performed simulations for sets, listed in table 1. Using $T_{\eta=\eta(t), \phi}$, we can check the existence of another SSFS which can not be reached by initial condition $S_{\text{in.}}$. In this case, we plot the sequence of the absolute value of the mean velocity $|\langle V \rangle_t|$; ($t = 0, T, 2T, \dots, T_{\text{end}} - T$). In all the analysis in this section, we fixed $\phi = 0$.

TABLE I: Table of the parameters for the definition of $\eta(t)$ (see (4.3)).

Run	η_1	η_2	η_3	t_1	t_2	t_3	t_4	T_{end}	symbol in fig.7
1	0.57	0.61	0.57	8T	30T	70T	92T	100T	+
2	0.60	0.64	0.60	8T	30T	70T	92T	100T	×
3	0.57	0.50	0.57	8T	30T	70T	92T	100T	*

2 Result

Fig.9 shows we have one state of non-zero mean velocity in the region $\eta > 1.0$. In this region, the mean velocity of the SSFS is almost independent of η . This is contrast to the averaged lift of the second flapping period shown in fig.5, in which the averaged lift shows a reduce around $\eta = 1.5$. Fig.9 shows \bar{V} is almost constant if $\eta > 1.0$. Again, this means that the interaction of two coherent vortices and wing are essential to achieve the SSFS (see sec.III). In the region $0.70 < \eta < 1.00$, the state is qualitatively the same as the state in the region $\eta > 1.0$, although the value of \bar{V} is not the same due to the short lifetime η .

To analyze the SSFS in the region $0.35 < \eta < 0.70$, we need the data obtained by $\langle V \rangle_t$, because there is another SSFS which can not be obtained by the simulation started from initial conditions (4.1). As well as \bar{V} , we regard the function $\langle V \rangle_t$ as (quasi-) SSFS, and plot them in fig.10.

In the region $0.57 < \eta < 0.61$, we see a SSFS characterized by zero-mean velocity by the result of *RUN 1* shown in fig.10 (except the first period due to the initial condition). However, it is suggested that the branch observed in the region $0.7 < \eta$ is also connected to another SSFS characterized by non-zero mean velocity. The result of *RUN 2* shows a transition from the SSFS characterized by zero-mean velocity to another SSFS characterized by non-zero mean velocity. In the initial eight period of these runs ($\eta = 0.60$), a SSFS characterized by zero-mean velocity is achieved, which is consistent with the case of *RUN 1*. However, after a transient state occurring when $\eta = 0.64$, (quasi-)SSFS converges to another SSFS characterized by non-zero mean velocity (about 0.12) in the last eight period in which $\eta = 0.60$ again.

If $\langle V \rangle_t$ after the transient state described above ($70T < t < 100T$) can be regarded as SSFS, their branch is close to a branch indicated by \bar{V} (where $\eta \geq 0.66$) shown in fig.10. We can see a long transient term for the run when η is near the critical point: in the region $0.53 < \eta < 0.55$, \bar{V} does not converge at $t = 30T$.

In the region $\eta < 0.35$, a single state of zero-mean velocity is observed. In this region, the SSFS is trivial: the flapping motion gives symmetric lift function without mean motion, as exemplified in section III.

3 Diagram

By knowledge of the functions \bar{V} and $|\langle V \rangle_t|$, we can construct the bifurcation diagram drawn in fig.11. The bifurcation diagram has mirror symmetry with respect to the line $\langle V \rangle = 0$ due to the symmetry of the system. There is a pitch-fork type bifurcation at **A** ($\eta \simeq 0.35$). In the region between **A** and **B** ($\eta \simeq 0.57$), there are one SSFS, **a**, characterized by $\langle V \rangle = \pm V_0 (\neq 0)$. These branches exist all the region where η is larger than **A**. In addition to that, the analysis in the above subsection, there is another SSFS characterized by $\langle V \rangle = 0$ between **B** and **C** ($\eta \simeq 0.62$). In this region, two SSFSs **a** and **b** coexist. Unstable mode is also shown, but they are one example deduced by the stable modes. SSFS **a** and **b** correspond to essentially different types of flapping dynamics. In the next section, we discuss the dynamics.

C. Dynamics of two flapping phases

In this subsection, we describe the dynamics of the two different SSFS. Parameter η is fixed 0.6 for achieving two different SSFS, which is obtained by *Run 2*: a sequence [7T, 8T] for zero-mean velocity state(**b** in fig.11), and a sequence [99T, 100T] for non-zero mean velocity state(**a** in fig.11).

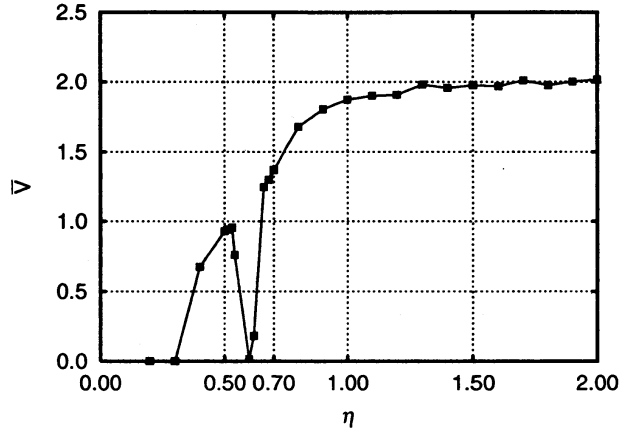


FIG. 9: Plotted graph of \bar{V} . In the region $\eta > 0.65$, \bar{V} has two stable states, while \bar{V} has a single mode in the region $\eta < 0.35$. In the region $\eta > 1.00$, \bar{V} takes almost the same value, which validates our cut-off viscosity method.

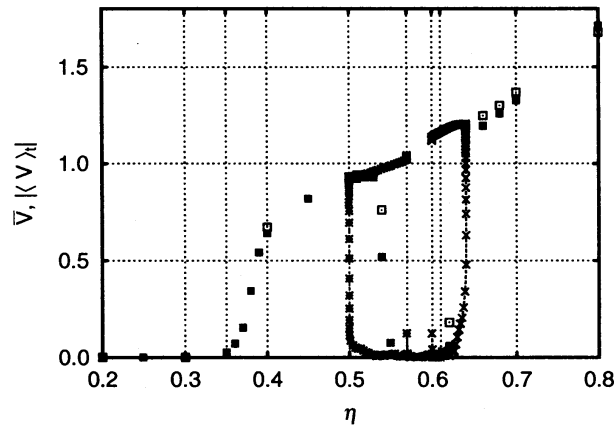


FIG. 10: Plotted graph of \bar{V} (open square is the run for $N = 50$ and filled square is the run for $N = 150$) and $\langle V \rangle_t$ in the region $0.20 < \eta < 0.80$. Function $\langle V \rangle_t$ is plotted as jointed-point graph. In the region $0.55 < \eta < 0.62$, two stable modes is observed.

Fig.12(a) and fig.12(b) shows two typical snapshots of zero-mean velocity state. The difference of their capture time is $1/2T$. The flow pattern and the distribution of point vortices are almost symmetric with respect to the horizontal line denoting the height of the center of mass. The symmetry of the relative position among point vortices and the wing results in the symmetric oscillation pattern in the phase space, which is shown in fig.13.

Because the value of η , 0.6, is sufficient for this model to form one coherent vortex, the coherent vortex shown in fig.12 works fully to generate lift. This interaction between one vortex and the wing is essential for lift production.

Fig.12(c) and fig.12(d) shows two typical snapshots of non-zero velocity state. The difference of their time is also $1/2T$. In this case, the flow pattern is asymmetric with respect to the horizontal line.

A coherent vortex is shown in the both figures, but the relative position of the vortex and the wing is different. In fig.12(c), the distance of the coherent vortex and the wing is small, which means strong lift generation. On the other hand, the distance is large in fig.12(d), and (negative) lift generation is small. This asymmetry causes an asymmetric shape of trajectory in the phase space shown in fig.13. However, it should be noted that the total sum of the instantaneous lift during one period is zero because of the definition of SSFS.

The magnitude of the parameter $\eta = 0.60$ is not sufficient to make a symmetry-breaking

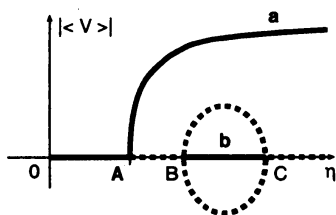


FIG. 11: Schematic picture of the bifurcation diagram. Solid line is a stable mode, and broken line is an example of unstable mode which is deduced by the structure of the stable mode.

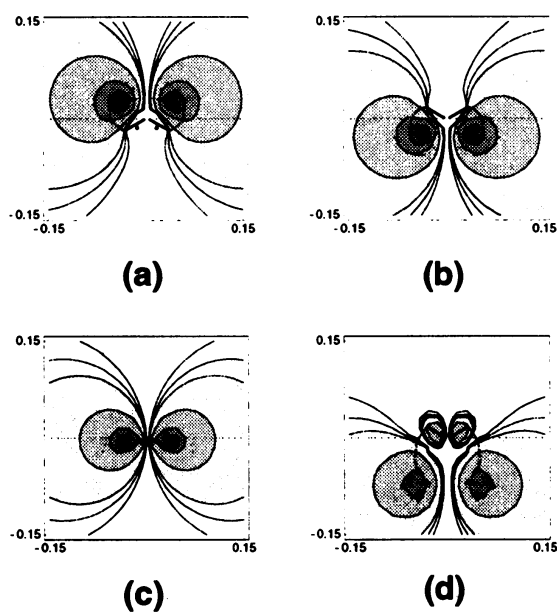


FIG. 12: Snapshots of the two SSFS in the case of $\eta = 0.60$. Horizontal broken line denotes the height of the center of mass. (a) State **b** (zero-mean); $t = 3/4T$ and (b) $t = 7/4T$: (a) and (b) are symmetric each other with respect to the horizontal line. (c) State **a** (non-zero mean); $t = 3/4T$ and (d) $t = 7/4T$:

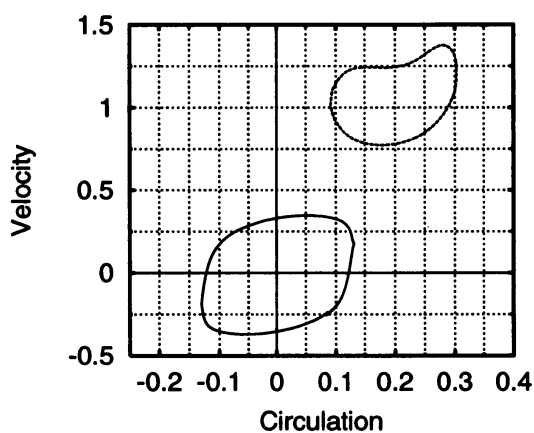


FIG. 13: Phase space of two SSFS for $\eta = 0.6$. Solid line corresponds to the SSFS characterized by zero-mean velocity. Broken line corresponds to the SSFS characterized by non-zero mean velocity.

dynamics discussed in sec.III. That is the reason why all the initial conditions of this case result in a symmetry state discussed in sec.IV A. On the other hand, SSFS characterized by non-zero mean velocity is achieved if $\eta > \eta_0 \simeq 0.62$. In this region, two coherent vortices interact with the wing, symmetry breaks, and all the initial conditions result in one non-zero mean velocity state.

The appearance of this dynamics is controlled by the nondimensional parameter η , and its occurrence is clearly separated at $\eta = \eta_0$. However, when this model is once locked in the non-zero mean velocity state, our result shows that the non-zero velocity state can be achieved even if $\eta < \eta_0$. One method to achieve the lock-in is to set η as a function of time, *i.e.*, Run 2. We can show a non-zero mean velocity state by a similar dynamics to that in sec. III even if η is constant and is smaller than η_0 . A method is to stop the flapping motion by changing $\theta(t)$ as

$$\theta(t) = \begin{cases} \Delta\theta \cos(2\pi t/T) & (t \leq 7T + \frac{1}{2}T, 8T + \frac{1}{2}T < t), \\ -\Delta\theta & (7T + \frac{1}{2}T < t \leq 8T + \frac{1}{2}T). \end{cases} \quad (4.4)$$

A stop of flapping in a temporal rising of CM causes a flow turning around wing. This flow helps to form a small coherent vortex under the wing. This small coherent vortex remains under the wing after the wing restarts flapping, and the dynamics of this vortex and another coherent vortex produced in the next downstroke becomes similar to the symmetry-breaking case.

V. CONCLUDING REMARKS

Our model, two plates attached together at a hinge, and flapping symmetric with respect to the horizontal line, shows interesting aspects of CM motion due to flapping. Given physical parameters, this model converges one or more discrete type(s) of steady periodic motion. Choosing a parameter η , the characteristic time of the cut-off viscosity in non-dimensional form, the stable state shows a bifurcation. The bifurcation diagram shows that i) a trivial state (zero-mean velocity) is not always stable; ii) two stable states can coexist in some region of η .

A dynamics which makes our model achieve the symmetry-breaking[18] is observed in a region $\eta > \eta_0 \simeq 0.62$, but the state characterized by non-zero mean velocity can be realized even if $\eta \leq \eta_0$. This means that the state characterized by non-zero mean velocity can be achieved by not only the typical dynamics shown in ref.[18] but another one. Long time simulations shows that the flapping state characterized by zero-mean velocity can be unstable, and that the model converges to a stable state characterized by non-zero mean velocity. Distinct dynamics to achieve the transition is not observed in this case.

The phenomena observed in the region $\eta < \eta_0$ might not be related to the 'real' situation, because our model simplifies viscosity. However, our simplified viscosity gives a relevant bifurcation parameter controlling the number of separated vortex. By this parameter, we can see a sharp change of the stable state characterized by zero-mean velocity and discuss the contribution of the coherent vortex directly. Thus it is easily known that the stability of the state is controlled by the amount of point vortices consisting of coherent vortex, contrary to the symmetry-breaking dynamics where the necessarily and sufficient condition of it is the coexistence of two coherent vortices.

In the standpoint of the the vortex-body interaction, this model presents a viewpoint of the analysis of these phenomena. The phase of the motion of the body interacting with fluid is classified as a function of nondimensional parameters [1, 2]. However, our model shows that given set of parameter does not always map into one type of motion. This result is meaningful when the dynamics of insect flight is considered, because they should choose a best type of flapping-flight mechanism corresponding to their circumstances. The existence of bistable mode in vortex-body interaction seems rather universal phenomenon: a similar behavior is observed in the case of one-dimensional flapping string in two-dimensional soap film [8].

Studies in terms of stability are required to understand phenomena related to the vortex-body interaction. To do that, a simple model with high-symmetry such as ours is quite useful, because classification of typical phenomena observed in vortex-body interactions is easy in this type of model and the classification is useful to analyse the vortex-body interaction.

REFERENCES

- [1] S. B. Field, M. Klaus, M. G. Moore, and F. Nori, *Nature* **388**, 252 (1997).
- [2] A. Belmonte, H. Eisenberg, and E. Moses, *Phys. Rev. Lett.* **81**, 345 (1998).
- [3] C. P. Ellington, *Amer. Zool.* **24**, 95 (1984).
- [4] C. P. Ellington, C. Berg, A. P. Willmott, and A. L. R. Thomas, *Nature* **384**, 626 (1996).
- [5] M. H. Dickinson, F.-O. Lehmann, and S. P. Sane, *Science* **284**, 1954 (1999).
- [6] A. P. Willmott and C. P. Ellington, *J. Exp. Biol.* **200**, 2705 (1997).
- [7] A. P. Willmott and C. P. Ellington, *J. Exp. Biol.* **200**, 2723 (1997).
- [8] J. Zhang, S. Childress, A. Libchaber, and M. Shelley, *Nature* **408**, 835 (2000).
- [9] Lamb, *Hydrodynamics, 6th Ed.* (Cambridge University Press, Cambridge, 1997).
- [10] H. Aref and S. W. Jones, *Phys. Fluids A* **5**, 3026 (1993).
- [11] A. P. Willmott, C. P. Ellington, and A. L. R. Thomas, *Phil. Trans. R. Soc. Lond. B* **352**, 303 (1997).
- [12] C. V. D. Berg and C. P. Ellington, *Phil. Trans. R. Soc. Lond. B* **352**, 317 (1997).
- [13] C. V. D. Berg and C. P. Ellington, *Phil. Trans. R. Soc. Lond. B* **352**, 329 (1997).
- [14] H. Liu and K. Kawachi, *J. Comp. Phys.* **146**, 124 (1998).
- [15] H. Liu, C. P. Ellington, E. Kawachi, C. V. D. Berg, and A. P. Willmott, *J. Exp. Biol.* **201**, 461 (1998).
- [16] Z. J. Wang, *Phys. Rev. Lett.* **85**, 2216 (2000).
- [17] Z. J. Wang, *J. Fluid Mech.* **410**, 323 (2000).
- [18] M. Iima and T. Yanagita, *J. Phys. Soc. Japan* **70**(1), 5 (2001).
- [19] M. Iima and T. Yanagita, in *Theoretical and Applied Mechanics* (the 50th Japan National Congress on Theoretical and Applied Mechanics, 2001), vol. 50, *to appear*.
- [20] S. Sunada, K. Kawachi, I. Watanabe, and A. Azuma, *J. Exp. Biol.* **183**, 217 (1993).
- [21] R. R. Clements, *J. Fluid Mech.* **57-2**, 321 (1973).
- [22] T. Inamuro, T. Adachi, and H. Sakata, in *Finite Element Flow Analysis*, edited by T. Kawai (University Tokto Press, Tokyo, 1982), pp. 931–938.
- [23] K. Takeda, O. R. Tutty, and A. D. Fitt, in *13th AIAA CFD Conference* (Colorado, 1997), pp. 97–1977.
- [24] S. Sunada, K. Kawachi, I. Watanabe, and A. Azuma, *J. Exp. Biol.* **183**, 249 (1993).